We are IntechOpen,
the world's leading publisher of
Open Access books
Built by scientists, for scientists

6,900
Open access books available

186,000
International authors and editors

200M
Downloads

Our authors are among the

154
Countries delivered to

TOP 1%
most cited scientists

12.2%
Contributors from top 500 universities

CLARIVATE ANALYTICS
BOOK CITATION INDEX
INDEXED

WEB OF SCIENCE™

Selection of our books indexed in the Book Citation Index
in Web of Science™ Core Collection (BKCI)

Interested in publishing with us?
Contact book.department@intechopen.com

Numbers displayed above are based on latest data collected.
For more information visit www.intechopen.com

Classical and Quantum Correspondence in Anisotropic Kepler Problem

Keita Sumiya, Hisakazu Uchiyama,
Kazuhiro Kubo and Tokuzo Shimada

Additional information is available at the end of the chapter

1. Introduction

If the classical behavior of a given quantum system is chaotic, how is it reflected in the quantum properties of the system? To elucidate this correspondence is the main theme of the quantum chaos study. With the advent of nanophysics techniques, this has become also of experimental importance. With the advent of new technology, various quantum systems are now challenging us. These include nano-scale devices, laser trapping of atoms, the Bose-Einstein condensate, Rydberg atoms, and even web of chaos is observed in superlattices.

In this note we devote ourselves to the investigation of the quantum scars which occurs in the Anisotropic Kepler Problem (AKP) – the classical and quantum physics of an electron trapped around a proton in semiconductors. The merit of AKP is that its chaotic property can be controlled by changing the anisotropy from integrable Kepler limit down ergodic limit where the tori are completely collapsed and isolated unstable periodic orbits occupy the classical phase space. Thus in AKP we are able to investigate the classical quantum correspondence at varying chaoticity. Furthermore each unstable periodic orbit (PO) can be coded in a Bernoulli code which is a large merit in the formulation of quantum chaos in term of the periodic orbit theory (POT) [1, 2, 6].

The AKP is an old home ground of the quantum chaos study. Its low energy levels were used as a test of the periodic orbit theory in the seminal work of Gutzwiller [3-7]. Then an efficient matrix diagonalization scheme was devised by Wintgen et al. (WMB method) [8]. With this method, the statistics of up to nearly 8000 AKP quantum levels were examined and it was found that the quantum level statistics of AKP change from Poisson to Wigner distribution with the increase of mass anisotropy [9]. Furthermore, an intriguing classical Poincaré surface of section (POS) was found at medium anisotropy ($\gamma \equiv m(\text{light})/m(\text{heavy}) = 0.8$),

which indicates remnants of tori (cantori) in the classical phase space [9]. Thus, over two decades from the early 70th, AKP was a good testing ground of theories (along with billiards) as well as a constant source of important information to quantum chaos studies. However, there has not been much recent theory investigation on AKP. Especially, to our knowledge, the quantum scar of the classical periodic orbits in AKP has not been directly examined, even though intriguing phenomena was discovered by Heller [10] in 1984. On the other hand, for an analogous system – the hydrogen under a magnetic field (diamagnetic Kepler problem (DKP)), the scars of periodic orbits were extensively studied using highly efficient tool called as scar strength functions [11]. We note that AKP is by far simpler; for DKP it is necessary to code the POs by a sequence of symbols consisting of three letters.

Recently the level statistics of AKP was examined from the random matrix theory view [12]. It was considered that the AKP level statistic in the transitive region from Poisson to Wigner distribution correspond to the critical level statistics of an extended GOE random matrix theory and it was conjectured that the wave functions should exhibit characteristic multifractality. This aspect has been further developed in [13, 14]; it is considered that *Anderson transition* occurs in the quantum physics of a class of physical systems such as AKP and periodically driven kicked rotator in their critical parameter regions. Further very recently a well devised new solid state experiment has been conducted for AKP and ADKP [15, 16]. We also refer [17] for a recent overview including this interesting conjecture.

Such is the case we have recently conducted AKP high accuracy matrix diagonalization based on the WMB method. This is not a perturbation calculation; the anisotropy term is not regarded as a perturbation and the full Hamiltonian matrix is diagonalized. Thus the approximation comes only from the size of the matrix. But, as a trade-off, a scaling parameter is unavoidably included; it is crucial to choose a correct parameter value at every anisotropy parameter. We have derived a simple rule of thumb to choose a suitable value [17]. After comparing with original WMB result in Sturmian basis, we have also worked with tensored-harmonic-wavefunction basis (THWFB) [11], which is more suitable for the Husimi function calculation to investigate the quantum scars. Our contribution here is the calculation of anisotropy term in the AKP Hamiltonian in THWFB [17], which is harder than the diamagnetic case. Comparing the results from two independent bases we have verified that both results agree completely thus the choices of scaling parameters (in both bases) are validated.

Aimed by these numerical data, we report in section 2 salient evidences of quantum scars in AKP for the first time. We compare the features of various known observables; thus this section will serve as a comparative test of methods and fulfills the gap in the literature pointed out above. Most interesting is the test using the scar strength function. We show that even in the ergodic regime ($\gamma = 0.2$), we can quantitatively observe that prominent periodic orbits systematically contribute to the quantum theory endowed with random energy spectrum.

In section 3 we investigate that how the scaring phenomena are affected by the variation of the anisotropy parameter. It is well known that the energy levels show successive avoiding crossings. On the other hand, in the periodic orbit formula, each term in the series for the density of states (DOS) consists of a contribution of an unstable PO with a pole (with an imaginary part given by the Lyapunov exponent of the PO) at the Bohr-Sommerfeld-type energy; thus each term smoothly varies with the anisotropy. We show that how these two

seemingly contradicting features intriguingly compromise. The localization patterns in the wave functions or Husimi functions are swapped between two eigenstates of energy at every avoiding crossing. Repeating successively this swap process characteristic scarring patterns follow the POs responsible to them. In this sense the quantum scarring phenomena are robust. We conclude in section 4.

2. Manifestation of Scars in AKP

We first explain how we have prepared the energy levels and wave functions. Then we introduce the indispensable ingredients to study the scars in AKP. After briefly explaining Husimi functions, we explain periodic orbit theory. The quantum scars will be observed along the classical unstable periodic orbits.

2.1. Matrix diagonalization

2.1.1. AKP Hamiltonian

The AKP Hamiltonian in the dimensionless form is given by

$$H_G = \frac{1}{2\mu}p_x^2 + \frac{1}{2\nu}(p_y^2 + p_z^2) - \frac{1}{r} \tag{1}$$

where $r = \sqrt{x^2 + y^2 + z^2}$ and $\mu > \nu$[1,4] with which POT was formulated in the history, or equivalently it may be also written as [9,11] (Harmonic basis)

$$H_W^{88} = \frac{1}{2}(p_x^2 + p_y^2) + \frac{\gamma}{2}p_z^2 - \frac{1}{r} \tag{2}$$

with $\gamma = \nu/\mu = 1/\mu^2$ or

$$H_W^{87} = p_x^2 + p_y^2 + \gamma p_z^2 - \frac{2}{r} \tag{3}$$

as used in WMB (Sturmian basis) [8]. We recapitulate POT predictions in terms of (1), our formula for AKP eigenvalue calculation in tensored harmonic wave function basis in terms of (2), and we discuss quantum scars using energy values in (3) in order to facilitate comparison with literature.

2.1.2. Matrix diagonalization in Sturmian basis

We here summarize WMB method for efficient matrix diagonalization.

Firstly, in the Sturmian basis

$$\langle \vec{r} | n\ell m \rangle = \frac{1}{r} \sqrt{\frac{n!}{(2\ell + n + 1)!}} e^{-\frac{\lambda r}{2}} (\lambda r)^{\ell+1} L_n^{2\ell+1}(\lambda r) Y_{\ell m}(\theta, \varphi) \tag{4}$$

with a scaling parameter λ, the Schrödinger equation of the AKP becomes a matrix equation:

$$\left[-\lambda \overleftrightarrow{\Delta^{(3)}} + (1-\gamma)\lambda \overleftrightarrow{\frac{\partial^2}{\partial z^2}} - 2\overleftrightarrow{\frac{1}{r}} \right] \boldsymbol{\Psi} = \frac{E}{\lambda} \overleftrightarrow{\mathrm{Id}} \, \boldsymbol{\Psi} \tag{5}$$

Dividing the whole equation by λ and packing E/λ^2 into a parameter ε, one obtains

$$\overleftrightarrow{M} \boldsymbol{\Psi} \equiv \left[-\overleftrightarrow{\Delta^{(3)}} + (1-\gamma)\overleftrightarrow{\frac{\partial^2}{\partial z^2}} - \epsilon \overleftrightarrow{\mathrm{Id}} \right] \boldsymbol{\Psi} = \frac{2}{\lambda} \boldsymbol{\Psi}. \tag{6}$$

This ϵ is to be fixed at some constant value. In principle any value will do, but for finite size of Hamiltonian matrix, the best choice is given [17] approximately

$$\varepsilon^* \simeq -\frac{1}{4}\gamma. \tag{7}$$

With this choice, we can get the largest number of reliable energy levels at a given matrix size. The ratio of reliable levels to the matrix size can be estimated as

$$R_{eff} \simeq \sqrt{\gamma}. \tag{8}$$

After fixing ε, the diagonalization of (6) is performed for $2/\lambda_i$ s and finally we obtain the energy eigenvalues by

$$E_i = \varepsilon \lambda_i^2. \tag{9}$$

2.1.3. Matrix diagonalization in Sturmian basis

For the (tensored) harmonic wave function basis (THWFB) [11] we convert the Hamiltonian of AKP into the Hamiltonian of two of two-dimensional harmonic oscillators.

For this purpose semi-parabolic coordinates are introduced

$$\mu\nu = \rho = \sqrt{x^2 + y^2}, \quad \frac{1}{2}(\mu^2 - \nu^2) = z, \quad \phi = \tan^{-1}\left(\frac{y}{x}\right) \tag{10}$$

and the AKP Schrödinger equation becomes

$$\left[-\frac{1}{2\left(\mu^2+\nu^2\right)}\left(\Delta_\mu^{(2)}+\Delta_\nu^{(2)}\right) + \frac{1-\gamma}{2}\frac{\partial^2}{\partial z^2} - \frac{2}{\mu^2+\nu^2} \right]|\Psi\rangle = E|\Psi\rangle. \tag{11}$$

Multiplying by $\mu^2+\nu^2$ and swapping the Coulombic interaction term and the E term one obtains

$$\left[-\frac{1}{2}\left(\Delta_\mu^{(2)}+\Delta_\nu^{(2)}\right) + |E|\left(\mu^2+\nu^2\right) + \frac{1-\gamma}{2}\left(\mu^2+\nu^2\right)\frac{\partial^2}{\partial z^2} \right]|\Psi\rangle = 2|\Psi\rangle. \tag{12}$$

Thanks to the semi-parabolic coordinates, the Coulombic singularity has removed [19] for $\gamma = 1$. Corresponding to the Sturmian basis with a scaling parameter λ in (4), we introduce the harmonic wave function basis

$$\langle \mu, \nu \mid i, j, \kappa \rangle = \frac{\kappa}{\pi} L_i(\kappa\mu^2) L_j(\kappa\nu^2) \exp\left(-\frac{\mu^2+\nu^2}{2} \right)$$

with a scaling parameter κ and, corresponding to ε in (6), we introduce a parameter

$$\tilde{\varepsilon} = 2\frac{|E|}{\kappa^2} \tag{13}$$

and we solve (12) after transforming it into the matrix equation of WMB form with eigenvalues $\Lambda_n = 2/\kappa_n$. The matrix element calculation of the mass anisotropy term in (12) is somewhat involved and we refer to [17] for detail. Energy levels are then determined by

$$E_n = -\frac{\kappa_n^2}{2}\tilde{\varepsilon} = -\frac{2}{\Lambda_n^2}\tilde{\varepsilon} \tag{14}$$

The best value of $\tilde{\varepsilon}$ is given by

$$\tilde{\varepsilon}^* \approx \gamma \tag{15}$$

which is similar to (7).

We have found precise agreement between our calculations by the Sturmian basis and by the harmonic oscillator basis which in turn validates our choices of scaling parameter ε and $\tilde{\varepsilon}$.

For the calculation of Husimi functions and scar strength function which uses Husimi functions, we use the THWFB since the projection of the basis functions to the Gaussian packets are easy to calculate [17].

2.2. Husimi function

Husimi function is defined via the scalar product of the wave function $|\psi\rangle$ with a coherent state(CHS) $|q_0, p_0\rangle$ of the system [11]:

$$W_\psi^{Hus}(q_0, p_0) = |\langle \psi \mid q_0, p_0\rangle|^2. \tag{16}$$

A detailed account is given in [17].

2.3. Periodic orbit theory

2.3.1. Periodic orbit theory and the density of state

Let us recapitulate Gutzwiller's periodic orbit theory [4,20]. The starting point is Feynman's path integral formula for the propagator of a particle from q' to q'' during the time interval 0 to T;

$$K(q'', q', T) \equiv \langle q''| \exp\left(-i\frac{H}{\hbar}T\right) |q'\rangle = \int_{q'}^{q''} D[q]\, e^{\frac{i}{\hbar}\int_0^T L(q,\dot{q},t)dt} \tag{17}$$

The Green function (response function) is given by the Fourier transformation of the propagator

$$G(q'', q', E) \equiv -\frac{i}{\hbar}\int_0^\infty dt e^{\frac{iEt}{\hbar}} K(q'', q', T)$$

where E has infinitesimally small imaginary part for convergence. Thus we have

$$G(q'', q', E) = \langle q''| \frac{1}{E + i\varepsilon - \hat{H}} |q'\rangle = -\frac{i}{\hbar}\int_0^\infty dt e^{\frac{iEt}{\hbar}} \left[\int_{q'}^{q''} D[q]\, e^{\frac{i}{\hbar}\int_0^T L(q,\dot{q},t)dt}\right] \tag{18}$$

By a stationary approximation we obtain a semiclassical formula for the Green function

$$\tilde{G}(q'', q', E) \simeq \sum_\Gamma A_\Gamma \exp(\frac{i}{\hbar}S_\Gamma - i\frac{\nu_\Gamma}{2}) \tag{19}$$

where Γ denotes a classically arrowed orbit, ν_Γ is the number of conjugate points on the orbit, and the amplitude A_Γ accounts for the Van Vleck determinant. Note that the principal function in (18) is changed into the action $S = \int_{q'}^{q''} pdq$ and the phase $i\pi/4$ from the stationary point approximation is shifted into A_Γ.

Now the density of states is given by

$$\rho(E) \equiv \sum_n \delta(E - E_n) = -\frac{1}{\pi}\mathrm{Im}\left(T_{r_n}\left(\frac{1}{E + i\varepsilon - \hat{H}}\right)\right) \tag{20}$$

where in the second equality an identity $1/(x + i\varepsilon) = P(1/x) - i\pi\delta(x)$ is used and trace is taken over all energy eigenstates $\{|n\rangle\}$. Trading this tracing with the tracing over the eigenstates of coordinate operator $\{|q\rangle\}$, we obtain a semiclassical approximation for the DOS

$$\rho(E) \approx -\frac{1}{\pi}\mathrm{Im}\int dq'\, \tilde{G}(q'', q', E)\big|_{q''=q'} = -\frac{1}{\pi}\mathrm{Im}\int dq' \sum_{\Gamma} A_{\Gamma} \exp\left(\frac{i}{\hbar}S_{\Gamma} - i\frac{\nu_{\Gamma}}{2}\right) \tag{21}$$

The integration over q' can be again approximated by a stationary phase approximation. Because

$$p'' = \frac{\partial S(q'', q')}{\partial q''}, \quad p' = -\frac{\partial S(q'', q')}{\partial q'} \tag{22}$$

the stationary phase condition gives

$$0 = \frac{\partial S(q', q')}{\partial q'} = p'' - p' \tag{23}$$

which dictates the periodic orbits. We obtain finally the periodic orbit theory formula for the DOS

$$\rho(E) \simeq \overline{\rho(E)} + \mathrm{Im} \sum_{r \in PO} \frac{T_r}{\pi\hbar} \sum_{n \neq 0} \frac{\exp\left\{in\left[\frac{S_r}{\hbar} - \frac{\pi}{2}l_r\right]\right\}}{[\det((M_r)^n - 1)]^{\frac{1}{2}}} \tag{24}$$

Here the first sum runs over all primitive POs and the n sum counts the repetitions of each peridic orbit; T_r, S_r, and l_r denote the period, action, and Maslov index of the primary PO, and the matrix M stands for the monodromy matrix of the primary PO.

In AKP $m = 0$ sector, the motion is restricted in a fixed plane which includes the heavy axis, and the problem essentially reduces to two dimensional one. (Later on the three dimensional feature is recovered only by the proper choice of the Maslov index [4]). As for AKP unstable periodic orbits, M has two eigenvalues e^u and e^{-u} (hyperbolic case) and the determinant in (24) is given by

$$\frac{1}{2}\left[\det(M^n - 1)\right]^{\frac{1}{2}} = -i\sinh(nu/2) \tag{25}$$

2.3.2. Naming of a periodic orbit

In AKP every PO can be coded by the sign of the heavy axis coordinate when the heavy axis is crossed by it. Note that number of the crossings must be even $(2n_c)$ for the orbit to close.

In this note we shall denote the PO according to Gutzwiller's identification number along with the Bernoulli sequence of POS. (See Table 1 in ref. [3] which gives a complete list[1] of POs up to $n_c = 5$ for the anisotropy $\gamma = 0.2$.) For instance, PO36($+ + - + + -$) is the identification number 6 among $n_c = 3$ POs.

2.3.3. The contribution of a periodic orbit to the density of state

The contribution of a single periodic orbit r to the DOS is estimated by a resummation of the sum over the repetition j (after the approximation $\sinh x \approx e^x/2$),

$$\rho(E)|_r \approx T_r \sum_m \frac{u_r \hbar/2}{(S_r - 2\pi\hbar(m + l/4))^2 + (u_r \hbar/2)^2} . \tag{26}$$

This gives Lorentzian peak at

$$S_r = 2\pi\hbar(m + l/4) \tag{27}$$

similar to the Bohr-Sommerfeld formula. In AKP the action S is given as

$$S_r(E) = \frac{T_r}{\sqrt{-2E}}. \tag{28}$$

Hence the peak position of the Lorentzian form in the energy is given by

$$E_{r,m} = -\frac{1}{2} \left(\frac{T_r}{2\pi\hbar(m+1)} \right)^2, \tag{29}$$

where Maslov index $l = 4$ for three dimensions is taken.

We are aware that it is meant by (24) that the exact DOS with sharp delta function peaks on the energy axis corresponds to the sum of all PO contributions [20] (assuming convergence).

It is the collective addition of all POs that gives the dos. But, still, it is amusing to observe that the localization of wave functions occurs around the classical periodic orbits as we will see below.

---

[1] In [3, 5] an amazing approximation formula that gives a good estimate of the action of each periodic orbit from its symbolic code is presented. The trace formula has a difficulty coming from the proliferation of POs of long length. This approximation gives a nice way of estimating the sum. The table is created to fix the two parameters involved in the approximation. We thank Professor Gutzwiller for informing us of this formula a few years ago.

2.4. Scars as observed in the probability distributions and Husimi functions

2.4.1. The manifestation of the fundamental FPO$(+-)$

Let us start exploring the scars in AKP first by investigating the case of the fundamental periodic orbit FPO $(+-)$ which reduces the Kepler ellipse orbit in the limit $\gamma = 1$.

In Figure 1, we show the wave function squared in the $\mu\nu$ plane and the Husimi distribution in the $\mu\,p_\mu$ plane. The FPO is shown by red line and compared with the probability distributions in the in the $\mu\nu$ plane. At high anisotropy the orbit is largely distorted. Still at chosen energy levels (upper row) we find clear localization around the FPO for both anisotropies. In the lower row we have displayed other energy eigenstates. For these energy levels we see also characteristic probability distribution patterns but not around FPO. Now let us look at the Husimi distributions. In case of energies in the upper diagrams we see very clearly that around the Poincaré section of the FPO (the fixed points) the Husimi functions show clear scars, while in the lower we see anti-scars, the Husimi density is very low at the fixed points. It is clear that Husimi functions are superior observables. In this demonstration of scars we have scanned thousands of energy eigenstates and picked examples. Next task is to use the ability of POT predictions (24) to locate the scaring levels.
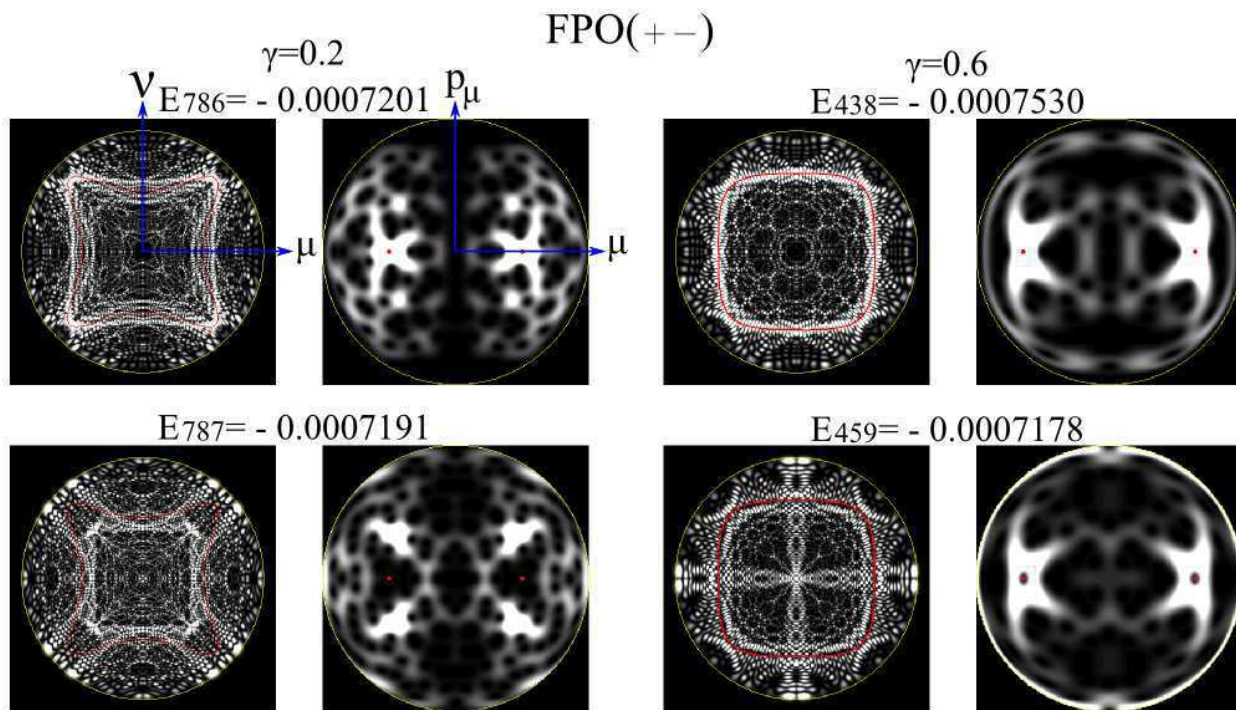

Figure 1. Scar and anti-scar phenomena with respect to the fundamental periodic orbit. The left set is for the anisotropy $\gamma = 0.2$ and right for $\gamma = 0.6$. In each set, the upper and lower row display prominent scar and anti-scar respectively, while the left and right columns exhibit the probability distribution on the $\mu\nu$ plane and Husimi distribution on the $\mu\,p_\mu$ plane ($\nu = 0$). The fundamental orbit is drawn by a red line on the $\mu\nu$ plane and its Poincaré section on the $\mu\,p_\mu$ plane by red points. The respective eigenvalues are $E_{786}, E_{787}, E_{438}, E_{459}$ in the m = 0, ℓ =even sector. Classical kinematical boundaries are shown by yellow circles.

2.4.2. PO prediction and AKP Scars

As for the FPO the POT works quite well. Thus for this test we have selected more complicated PO PO22 $(+++-)$ and PO36 $(++-++-)$. These orbits wind around the heavy axis forth and back and presumably correspond to the bounce orbit in the billiard.[2] The top row in Fig.2 shows the prediction from POT – the contribution of the single orbit to the DOS (26). We observe clearly the peak regions of POT prediction contains at least one energy eigenstate which shows the scar of the orbit. On the other hand we have checked that the relevant orbit pattern does not appear in the non-peak region of the POT prediction.

In this analysis the Husimi function again yields unmistakable information on the scaring.

Figure 2. $\gamma = 0.6$, $l =$ even, $m = 0$. The upper diagrams: The red and green curves are contributions to the density of states $\rho(E)$ from bouncing-type periodic orbits PO22 $(+++-)$ and PO36 $(++-++-)$ respectively and the peak positions are compared with the l even $m = 0$ energy levels from matrix diagonalization (WMB with tensored harmonic oscillator basis). The lower: The quantum scars of these periodic orbits are exhibited on the probability distributions and the Husimi functions. (cf. Fig. 1).

[2] We thank Professor Toshiya Takami for explaining his articles [21,22] and pointing us this point.

2.5. Scars as analyzed by the scar strength function

2.5.1. Scar strength functions

In an extensive analysis of scars in the diamagnetic hydrogen, a tool called as scar strength function (SSF) is presented [11]. It is defined as

$$I_n^{PO} = \oint_{PO} d^4s \, W_{\psi_n}^{Hus} \left(\mu, \nu, p_\mu, p_\nu \right) \left(\oint_{PO} d^4s \right)^{-1}$$

where the integral is to be performed along the PO with $d^4s = \sqrt{d\mu^2 + d\nu^2 + dp_\mu^2 + dp_\nu^2}$. This quantity is exploiting to what extent a given PO is inducing localization along it in the Husimi function of a given energy eigenstate. Then spectral scar strength function is introduced as

$$I^{PO}(E) = \sum_n I_n^{PO} \delta \left(E - E_n \right)$$

This shows how the given PO affects each energy eigenstate in one function.

2.5.2. The use of SSF $I^{PO}(E)$

Let explore the region of high anisotropy ($\gamma = 0.2$) where the classical phase space is occupied by the unstable periodic orbits and chaoticity is rather high. We explore this region by the ability of $I^{PO}(E)$.

We start from FPO $(+-)$ in Fig. 3. The upper is the POT prediction curve, the middle is the SSF along with real eigenvalues and the bottom is as usual a direct comparison of FPO with wavefunctions squared as well as Husimi functions. The SSF is the quantum measure of scaring of a particular PO in consideration, while the FPO prediction is composed from purely classical information for the PO. When the curve of the contribution from a PO peaks, the SSF either peaks or reaches its minimum (10^{-10}). The agreement in the energy values of the peaks (or dips) is quite remarkable. But we do not know why anti-scar occurs here. This anti-scar is interesting in that it produces a bright hallow just of the same size and position of the scar but the central core is missing.

2.5.3. $I^{PO}(E)$ for various POs and their Fourier transform

Let us now examine the case of several POs simultaneously in Fig. 4. The profiles, the SSF, and the Fourier transforms to the action space are listed in three columns. As Wintgen et al. write as 'the scars are the rules rather than exception' [11] we find that particular energy eigenstates give salient high scar function value while the other states give very low value of order even 10^{-10}. Further more the Fourier transform $I^{PO}(S)$ of $I^{PO}(E)$ shows sequential peaks at equal ΔS. We compare in Fig. 5 ΔS_r^{QM} and S_r^{Cl} (the measured spacing of the orbit and the action of the PO). They agree excellently; the POs live in quantum theory.
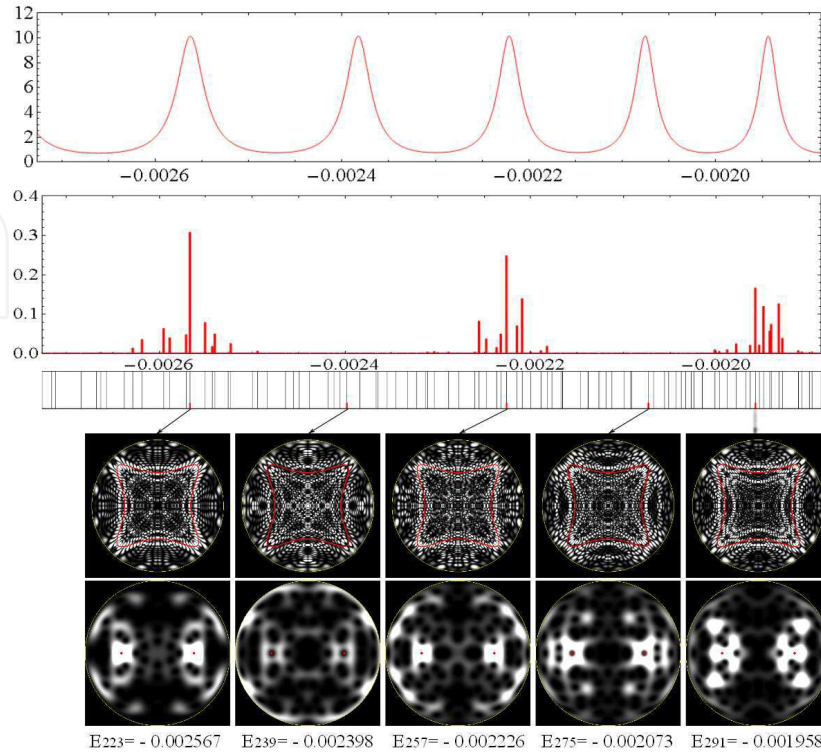
Figure 3. Contribution of FPO $(+-)$ to AKP. Upper two diagrams: The $(+-)$ contribution as a function of energy predicted by POT compared with the scar strength extraction from each of the energy eigenstates. Lower two diagrams: the scaring status of $(+-)$ at levels indicated by arrows are exhibited with respect to wave functions squared and Husimi functions. (cf. Fig. 1 and Fig. 2). Scar and anti-scar appear alternatively.

2.6. Direct phase space observation of Scaring orbit

The scar strength function is a useful tool which gives a list of numerical values which shows succinctly to which eigenstates the periodic orbit exerts its effect strongly. But we certainly want also visualized picture how the PO turns up in the 4 dimensional phase space. (Because $H = $ const., the actual independent variables are three, and we choose μ, ν, p_μ.) The sample pictures are shown in Fig.6.

3. Robustness of Scaring under the Variation of Anisotropy Parameter

3.1. Swap of the patterns under avoiding crossings

It is well known that the patterns of wave functions (and of Husimi distributions) are swapped between the energy eigenstates via the avoiding level crossings, which is easy to demonstrate in terms a simple coupling model of two levels. Fig. 7 is a typical example of this phenomenon.

It is shown in [21,22] that with the aid of the diabatic transformation one can trace the localization on the transformed basis until very near to the minimum gap with an explicit evidence in the billiard scars. We have verified this issue in AKP. Furthermore it is conjectured that the long periodic orbits may interpolates two shorter orbits and they may be the cause of the avoiding crossings in this way. We are testing this conjecture in AKP.
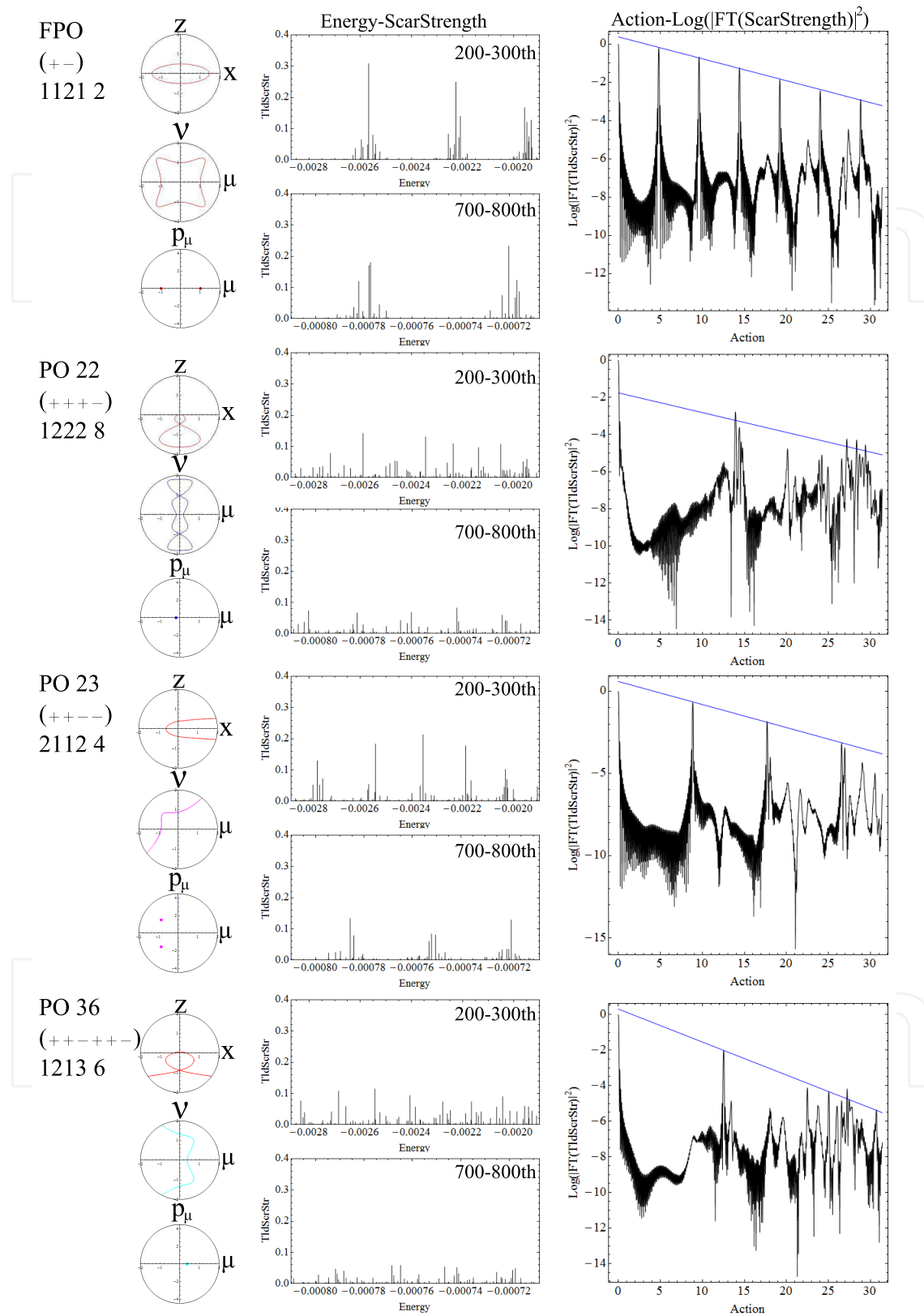
Figure 4. $\gamma = 0.2$ Profiles of PO, the scar strength function, and Fourier transformation of scar strength function to the action space.
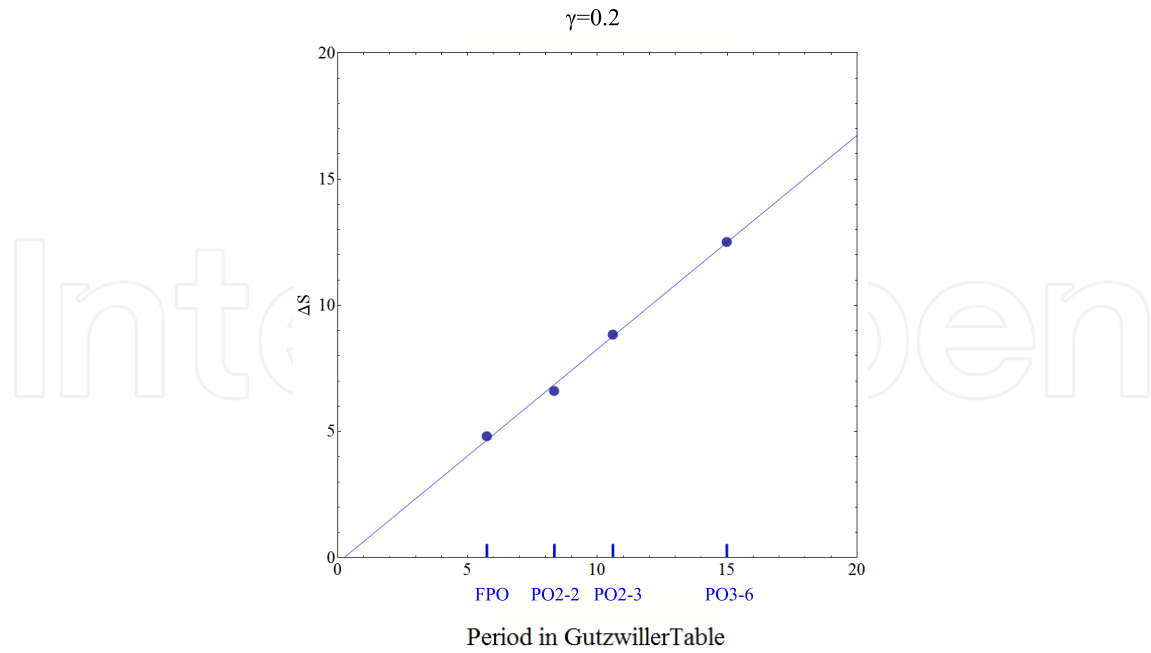
Figure 5. Plot of $(\Delta S_r^{QM}, S_r^{Cl})$ for periodic orbits r = FPO, PO22, PO23, PO36, where ΔS_r^{QM} is measured from the third column of Fig.4 and S_r^{Cl} is the action value of the classical orbit.
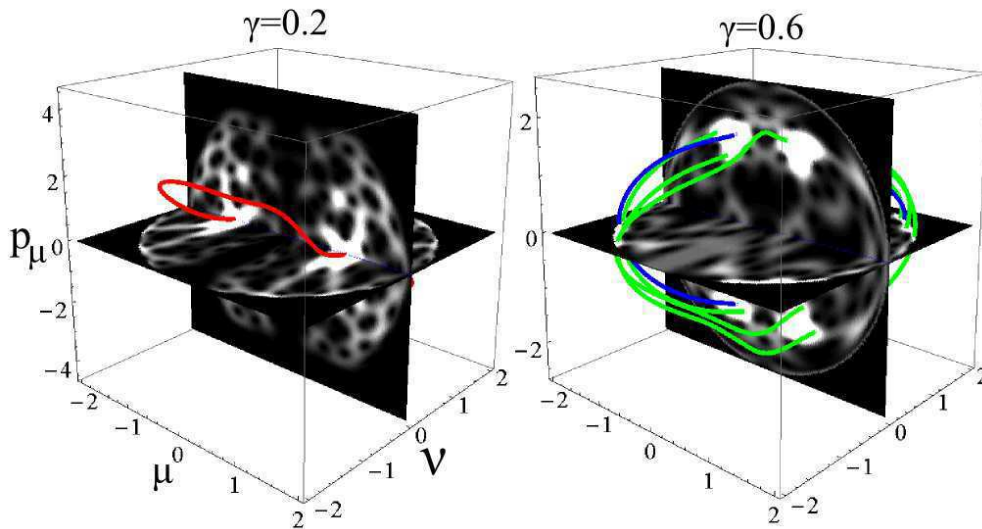

Figure 6. Two samples of density plot of Husimi functions in the 3 dimensional $\mu - \nu - p_\mu$ space. Left: γ =0.2, W_{Hus} for $E_{786} = -0.0007201$. Red orbit is the FPO $(+-)$. Right: γ=0.6, W_{Hus} for $E_{579} = -0.0005681$. Blue and green orbits are respectively PO23 $(+ + --)$ and PO37 $(+ + - - + -)$.

3.2. Robust association of localization with periodic orbits

We have posed the following question in the introduction of this chapter.

1. Energy levels exhibit randomness at high anisotropy and change *their values randomly* repeating successive avoiding crossings when the anisotropy parameter is varied gradually.
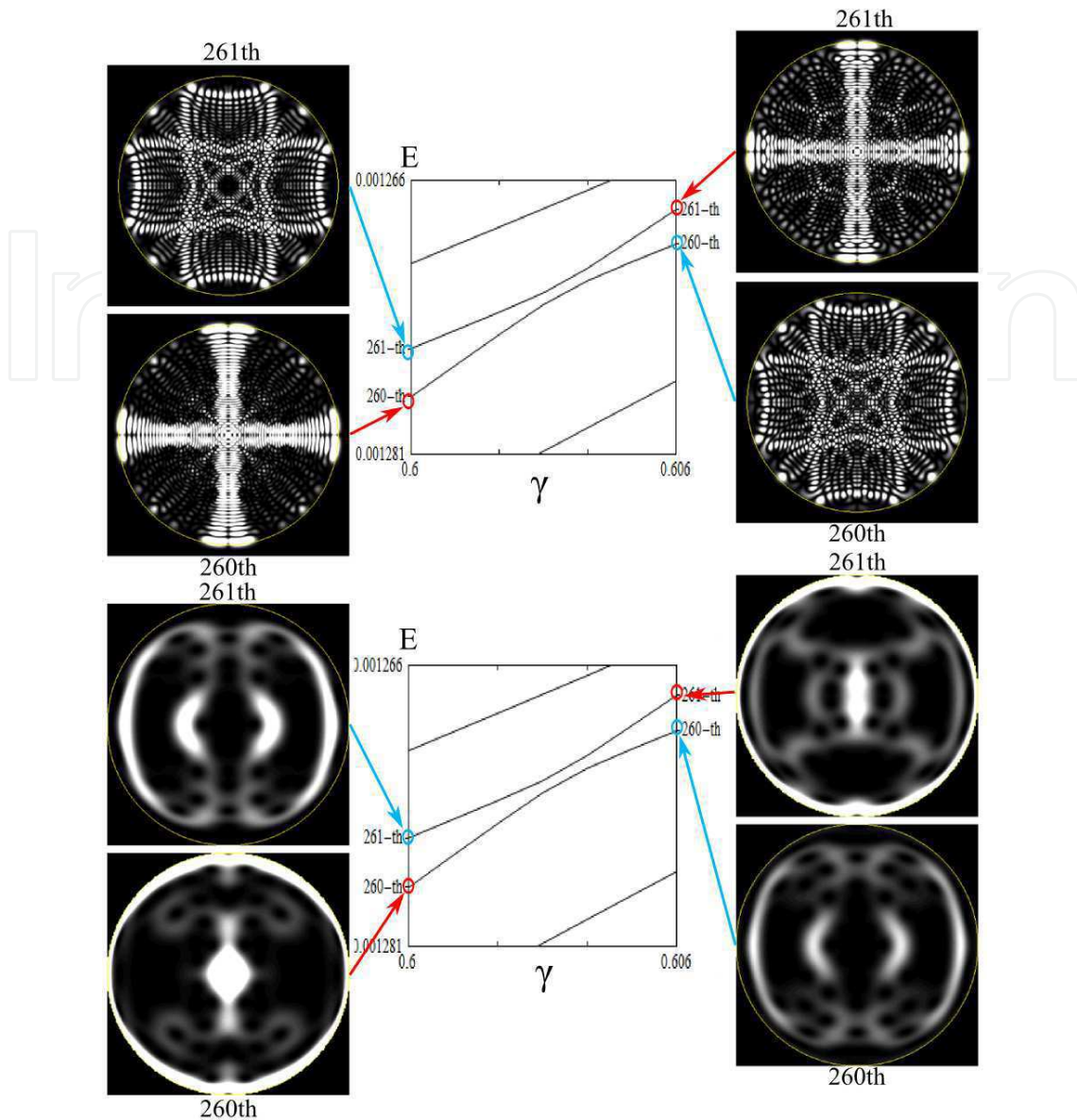
Figure 7. Avoiding level crossing between 260th and 261th energy eigen states under the variation of the anisotropy $\gamma \in [0.6, 0.606]$. Both the wave function squared and Husimi functions are swapped around the avoiding crossing.

2. On the other hand the peak locations (29) of the DOS as predicted by a single PO *change smoothly* with the anisotropy and the scar tends to be observed in the energy eigenstate around the peak position in the DOS as in Fig.2.

Aren't the two issues in contradiction? We have found that they can live together (within approximation of the fluctuation size). Most important point is that the swap of the localization patterns at avoiding crossing is in harmony with the transportation of them by the responsible PO orbits. Besides the POT prediction (29) does not imply the exact location of theappearance of the scar.

It has some allowance as recognized by the width of the *modulation* of SSF[11].

Let us explain this by Fig. 8. Here the anisotropy γ is varied from 0.6 to 0.7 with inclement 0.001. As for (1) we indeed observe both random fluctuation of energy levels as well as many

avoided crossings. As for (2), we have picked the bouncing-type periodic orbit PO22 as an example. The predicted peak position (29) of its contribution to DOS varies with the change of γ as shown by a red (almost straight) curve. This PO22 produces a salient *cross-shaped scar* at E_{260} (and E_{275}) at γ=0.6. We have investigated how the cross-shaped scar travels in the spectrum space suffering many avoiding crossings. It reaches at E_{276} (and E_{291}) at γ =0.7
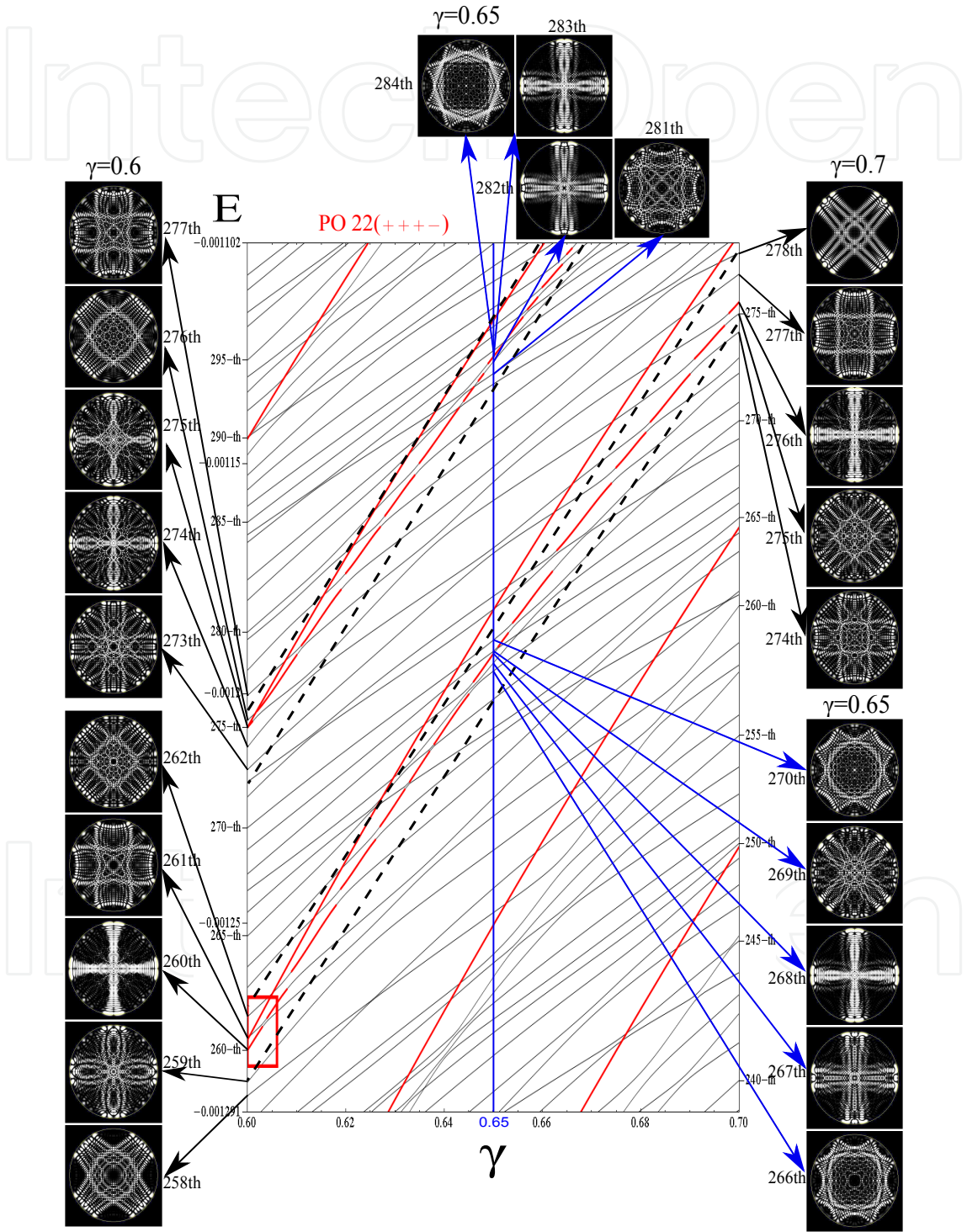

Figure 8. The spectrum lines in the wide interval $\gamma \in [0.6, 0.7]$ investigated with increment 0.001. The cross-shaped scar by PO22 travels within a belt bounded by two dashed lines. The POT prediction (24) is exhibited by a red curve.

and the track in between is enclosed by a belt shown by two dashed lines. We clearly observe that the belt is closely associated by the POT prediction curve. In this sense the association is robust.

4. Conclusion

We have presented ample examples of scaring phenomena for the first time in AKP. Especially we have found how the fluctuation of energy levels and smooth POT prediction for the scaring levels are compromised by using the advantage of AKP endowed by a chaoticity changing parameter.

Although the theme is old, the scaring phenomenon is fascinating and we hope this contribution fulfills a gap in the literature.

Acknowledgement

Author details

Keita Sumiya, Hisakazu Uchiyama,
Kazuhiro Kubo and Tokuzo Shimada

Department of Physics, School of Science and Technology, Meiji University, Japan

References

[1] Gutzwiller, M. C. (1977). Bernoulli sequences and trajectories in the anisotropic Kepler problem, Journal of Mathematical Physics 18: 806-823.

[2] Devaney, R. L. (1979). Collision Orbits in the Anisotropic Kepler Problem, Inventions math. 45: 221-251.

[3] Gutzwiller, M. C. (1981). Periodic orbits in the anisotropic Kepler problem, in Devaney, R. L. & Nitecki, Z. H. (ed.) Classical Mechanics and Dynamical systems, Marcel Dekker, New York, pp. 69-90.

[4] Gutzwiller, M. C. (1971). Periodic orbits and classical quantization conditions, Journal of Mathematical Physics 12: 343-358.

[5] Gutzwiller, M. C. (1980). Classical quantization of a hamiltonian with ergodic behavior, Physical Review Letters 45: 150-153.

[6] Gutzwiller, M. C. (1982). The quantization of a classically ergodic system, Physica D 5: 183-207.

[7] Gutzwiller, M. C. (1990). Chaos in Classical and Quantum Mechanics, Springer.

[8] Wintgen, D., Marxer, H. & Briggs, J. S. (1987). Efficient quantisation scheme for the anisotropic Kepler problem, Journal of Physics A 20: L965-L968.

[9] Wintgen, D. & Marxer, H. (1988). Level statistics of a quantized cantori system, Physical Review Letters 60: 971-974.

[10] Heller, E. J. (1984). Bound-state eigenfunctions of classically chaotic hamiltonian systems: scars of periodic orbits, Physical Review Letters 53: 1515-1518.

[11] Müller, K. & Wintgen, D. (1994). Scars in wavefunctions of the diamagnetic Kepler problem, Journal of Physics B: Atomic, Molecular and Optical Physics 27: 2693-2718.

[12] García-García, A. M. & Verbaarschot, J. J. M. (2003). Critical statistics in quantum chaos and Calogero-Sutherland model at finite temperature, Physical Review E 67: 046104-1 -046104-13.

[13] García-García, A. M. (2007). Universality in quantum chaos and the one parameter scaling theory (a power point of a talk). http://www.tcm.phy.cam.ac.uk/ amg73/oslo2007.ppt.

[14] García-García, A. M. & Wang, J. (2008). Universality in quantum chaos and the one-parameter scaling theory, Physical Review Letters 100: 070603-1 - 070603-4.

[15] Chen, Z. et al. (2009). Realization of Anisotropic Diamagnetic Kepler Problem in a Solid State Environment , Physical Review Letters 102: 244103.

[16] Zhou, W. (2010). Magnetic Field Control of the Quantum Chaotic Dynamics of Hydrogen Analogues in an Anisotropic Crystal Field, Physical Review Letters 105: 024101.

[17] Kubo, K. & Shimada, T. (2011). Theoretical Concepts of Quantum Mechanics, InTech.

[18] Kustaanheimo, P. & Stiefel, E. (1965). Perturbation theory of Kepler motion based on spinor regularization, Journal für die reine und angewandte Mathematik 218: 204-219.

[19] Husimi, K. (1940). Some formal properties of the density matrix, Proceedings of the Physico-Mathematical Society of Japan 22: 264-314.

[20] Wintgen, D. (1988). Semiclassical Path-Integral Quantization of Nonintegrable Hamiltonian Systems, Physical Review Letters 61: 1803-1806.

[21] Takami, T. (1992). Semiclassical Interpretation of Avoided Crossings for Classically Nonintegrable Systems, Physical Review Letters 68: 3371-3374.

[22] Takami, T. (1995). Semiclassical study of avoided crossings, Physical Review E 52: 2434.